LA-UR- 09-01473

Approved for public release; distribution is unlimited.

Title:	On the model discriminating power of mu to e conversion in nuclei
Author(s):	Vincenzo Cirigliano, T-2 Ryuichiro Kitano, T-2 Yashuiro Okada, Tsukuba KEK Theory Group, Japan Paula Tuzon, Universitate de Valendic, Spain
Intended for:	Phys. Rev. D

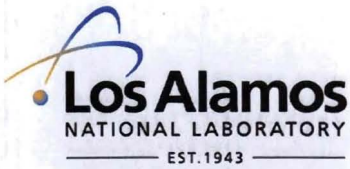

Form 836 (7/06)

LA-UR-09-????

On the model discriminating power of $\mu \to e$ conversion in nuclei

Vincenzo Cirigliano[a], Ryuichiro Kitano[a], Yashuiro Okada[b], Paula Tuzon[a,c]

[a] *Theoretical Division, Los Alamos National Laboratory, Los Alamos, NM 87545, USA*

[b] *Theory Group, KEK, Oho 1-1, Tsukuba, Ibaraki 305-0801, Japan and Department of Particle and Nuclear Physics, The Graduate University for Advanced Studies, Oho 1-1, Tsukuba, Ibaraki 305-0801, Japan*

[c] *Departament de Física Teòrica, IFIC, CSIC — Universitat de València Edifici d'Instituts de Paterna, Apt. Correus 22085, E-46071 València, Spain*

Abstract

Contents

Things to refine/complete:

- **Introduction**
- **Throughout, add (or complete) the relevant references.**
- **Axes labels in the plots.**
- **Section on SUSY see-saw**
- **Conclusions**

1 Introduction

Here are some items that could be expanded in a more complete introduction:

- Lepton Flavor Violating (LFV) charged lepton decays provide a highly sensitive probe of physics beyond the Standard Model (SM), due to the un-observably small branching fractions ($\sim 10^{-50}$) predicted for these modes in the SM (minimally extended to include massive neutrinos). Searches for SM forbidden muon processes, such as $\mu \to e\gamma$, $\mu \to e\bar{e}e$, and $\mu \to e$ conversion in nuclei, have provided so far the strongest constraints on LFV new physics. This statement can be characterized in a model-indepenent way as a lower bound on the scale associated to a set of dimension six effective operators parameterizing new physics beyond the SM. [**Add numbers here**].

- It is a well known fact that while the decay $\mu \to e\gamma$ is only sensitive to a transition magnetic dipole operator, both $\mu \to e\bar{e}e$ and $\mu \to e$ conversion in nuclei are sensitive to transition charge radii operators as well as purely contact four-fermion interactions induced by physics beyond the SM. In other words, different LFV decays have different sensitivities to underlying LFV mechanisms (effective operators). This leads naturally to ask the question whether one could infer the relative strength of these different operators in a completely phenomenological and model-independent way This would allow one to discriminate among different underlying models of LFV and thus would provide valuable input for model building.

- In Ref. [1] it was pointed out that in principle, by combining the rates of $\mu \to e\gamma$ and $\mu \to e$ conversion on different target nuclei, one could discriminate underlying models. [**Here add a simple discussion of Z-dependence of overlap integrals as due to relativistic effects**]

- In this work we go back to this issue with the aim to
  - quantify the theoretical uncertainty induced by the hadronization process;
  - quantify the experimental precision required to realistically infer useful information on the underlying LFV mechanisms.

  We organize our discussion as follows: in Section 2 we review the derivation of the $\mu \to e$ conversion rate starting from a general effective theory description of the LFV physics. In Section 3 we explore the phenomenological consequence of the simplest possible models, in which only one effective LFV operator dominates. We extend this analysis in Section 4 to the class of models in which two operators dominate. In Section 5 we specialize our discussion the SUSY see-saw model and summarize the conclusions of our analysis in Section 6.

2 LFV effective interaction and the $\mu \longrightarrow e$ conversion rate

In this section we review the procedure to calculate the rate of the $\mu \longrightarrow e$ conversion in nuclei, starting from a general parameterization of new physics effects via effective operators at a scale Λ larger than the electroweak scale $v \simeq 176$ GeV.

2.1 Weak scale effective lagrangian

We start with the most general effective Lagrangian which describes LFV transitions between charged leptons of first and second families at the weak scale:

$$\begin{aligned}
\mathcal{L}_{eff}^{(q)} &= -\frac{1}{\Lambda^2}\Bigg[\left(C_{DR} m_\mu\, \bar{e}\sigma^{\rho\nu}\mathcal{P}_L\mu + C_{DL} m_\mu\, \bar{e}\sigma^{\rho\nu}\mathcal{P}_R\mu\right) F_{\rho\nu} \\
&+ \sum_q \left(C_{VR}^{(q)}\, \bar{e}\gamma^\rho P_R\mu + C_{VL}^{(q)}\, \bar{e}\gamma^\rho P_L\mu\right)\bar{q}\gamma_\rho q \\
&+ \sum_q \left(C_{SR}^{(q)} m_\mu m_q G_F\, \bar{e}\mathcal{P}_L\mu + C_{SL}^{(q)} m_\mu m_q G_F\, \bar{e}\mathcal{P}_R\mu\right)\bar{q}q \\
&+ \left(C_{GR} m_\mu G_F\, \bar{e}\mathcal{P}_L\mu + C_{GL} m_\mu G_F\, \bar{e}\mathcal{P}_R\mu\right)\frac{\beta_H}{2g_H^3} G_a^{\rho\nu} G^a_{\rho\nu} + h.c.\Bigg] \qquad (1)
\end{aligned}$$

In the above expression Λ represents the scale where new physics effects appear. The C_{AB}'s are dimensionless constants containing information about the underlying theory; the subindexes R, L correspond to the chirality of the final electron which is determined by $P_{R,L} = \frac{1\pm\gamma^5}{2}$, q are light and heavy quarks, $F_{\rho\nu} = \partial_\rho A_\nu - \partial_\nu A_\rho$, $G^a_{\rho\nu} = \partial_\rho G^a_\nu - \partial_\nu G^a_\rho - f_{abc} G^b_\rho G^c_\nu$, $\sigma^{\rho\nu} = \frac{i}{2}[\gamma^\rho, \gamma^\nu]$. $G_F = 1/v^2$ is the Fermi constant, while m_μ and m_q represent the muon and quark masses, respectively. β is the usual β-function defined as $\mu\frac{dg}{d\mu} \equiv \beta(g)$, where g is the strong coupling constant. The notation $g_{H,L}$ and $\beta_{H,L}$ is used to differentiate the Lagrangian with all quarks contributions (H) from the one where heavy quarks are integrated out (L). This Lagrangian describes three kind of interactions that violate the lepton flavor: The effective interaction with a photon (Dipole term), the effective interaction with quarks (Scalar and Vector terms) and the effective interaction with gluons (Gluon term).

2.2 Integrating out heavy quarks

At lower energies where heavy quarks are integrated out, their contribution in the Scalar term can be parametrized through the Gluon term. The physical quantity used to do the

matching is the energy-momentum tensor, that at high energies can be written as

$$\theta^\alpha_\alpha = \sum_{q'=u,d,s} m_{q'}\ \bar{q}'q' + \sum_{Q=c,t,b} m_Q\ \bar{Q}Q + \frac{\beta_H}{2g_H^3} GG\ , \tag{2}$$

where the contributions of light and heavy quarks are separated and GG stands for $G^{\rho\nu}_a G^a_{\rho\nu}$. The same expression can be written for different number of existing quarks,

$$\begin{aligned}
\theta^\alpha_\alpha &= \sum_{q'=u,d,s} m_{q'}\ \bar{q}'q' + \sum_{Q'=c,b} m_{Q'}\ \bar{Q}'Q' + x_5\ GG \\
\theta^\alpha_\alpha &= \sum_{q'=u,d,s} m_{q'}\ \bar{q}'q' + \sum_{Q''=c} m_{Q''}\ \bar{Q}''Q'' + x_4\ GG \\
\theta^\alpha_\alpha &= \sum_{q'=u,d,s} m_{q'}\ \bar{q}'q' + x_3\ GG\ .
\end{aligned} \tag{3}$$

$x_i \equiv \frac{\beta_i}{2g_i^3}$ corresponds to the energy-momentum tensor relation when i flavors are entering and $6-i$ have been integrated out. The matching conditions read

$$\begin{aligned}
x_5\ GG &= m_t\ \bar{t}t + x_6\ GG \\
x_4\ GG &= m_t\ \bar{t}t + m_b\ \bar{b}b + x_6\ GG \\
x_3\ GG &= m_t\ \bar{t}t + m_b\ \bar{b}b + m_c\ \bar{c}c + x_6\ GG\ .
\end{aligned} \tag{4}$$

Taking into account (4), after integrating out the heavy quarks the Lagrangian is:

$$\begin{aligned}
\mathcal{L}^{(q')}_{eff} &= -\frac{1}{\Lambda^2}\Bigg[\left(C_{DR} m_\mu\ \bar{e}\sigma^{\rho\nu}\mathcal{P}_L\mu + C_{DL} m_\mu\ \bar{e}\sigma^{\rho\nu}\mathcal{P}_R\mu\right) F_{\rho\nu} \\
&+ \sum_{q=q'} \left(C^{(q)}_{VR}\ \bar{e}\gamma^\rho P_R\mu + C^{(q)}_{VL}\ \bar{e}\gamma^\rho P_L\mu \right) \bar{q}\gamma_\rho q \\
&+ \sum_{q=q'} \left(C^{(q)}_{SR} m_\mu m_q G_F\ \bar{e}\mathcal{P}_L\mu + C^{(q)}_{SL} m_\mu m_q G_F\ \bar{e}\mathcal{P}_R\mu \right) \bar{q}q \\
&+ \left(C_{GQR} m_\mu G_F\ \bar{e}\mathcal{P}_L\mu + C_{GQL} m_\mu G_F\ \bar{e}\mathcal{P}_R\mu\right) \frac{\beta_L}{2g_L^3} G^{\rho\nu}_a G^a_{\rho\nu} + h.c. \Bigg]
\end{aligned} \tag{5}$$

The Gluon term is written in terms of β_L and g_L, and the constants C_{GR} and C_{GL} have been changed to C_{GQR} and C_{GQL} respectively, to include the heavy quark contribution

$$\begin{aligned}
C_{GQR} &= \sum_Q C^{(Q)}_{SR}\ \kappa_{(Q)} + C_{GR}\kappa \\
C_{GQL} &= \sum_Q C^{(Q)}_{SL}\ \kappa_{(Q)} + C_{GL}\kappa\ ,
\end{aligned} \tag{6}$$

with $\kappa \equiv \frac{x_6}{x_3} = \frac{\beta_H}{\beta_L}\frac{g_L^3}{g_H^3}$, $\kappa_{(c)} \equiv \frac{x_3 - x_4}{x_3}$, $\kappa_{(b)} \equiv \frac{x_4 - x_5}{x_3}$ and $\kappa_{(t)} \equiv \frac{x_5 - x_6}{x_3}$, and each x_i reads (to one loop):

$$x \equiv \frac{\beta}{2g^3} = -\frac{1}{2(16\pi^2)}\left[\frac{11}{3}C_2(G) - \frac{4}{3}T(R)\right] , \tag{7}$$

being $C_2(G) = 3$ and $T(R) = \frac{1}{2}N_F$, where N_F is the number of flavors, tells us that $x_i - x_{i+1} = -\frac{1}{3}\frac{1}{16\pi^2}$, and so: $\kappa_{(Q)} = 0.07$ and $\kappa = 0.78$.

2.3 Nucleon level effective lagrangian

The Lagrangian (5) can be evolved witht he renormalization group down to energy scales of the order of $\mu \sim 1$ GeV. At this low scale, the effective lagrangian has to be written in terms of the relevant degrees of freedom, namely nucleons, leptons, and photons. Hadronic matrix elements of the operators $m_q\bar{q}q$, $\bar{q}\gamma_\rho q$ and $\frac{\beta_L}{2g_L^3}GG$ can be written as

$$\begin{aligned}
\langle N|m_q\bar{q}q|N\rangle &= m_N\, f_{SN}^{(q)}\, \bar{\psi}_N\psi_N \\
\langle N|\bar{q}\gamma_\rho q|N\rangle &= f_{VN}^{(q)}\, \bar{\psi}_N\gamma_\rho\psi_N \\
\langle N|\frac{\beta_L}{2g_L^3}GG|N\rangle &= m_N\, f_{GN}\, \bar{\psi}_N\psi_N ,
\end{aligned} \tag{8}$$

where N represents each nucleon ($N = p, n$) , ψ_N are the nucleon momentum-space wave-functions, and $f's$ are nucleon form factors. The latter depend in principle on the momentum transfer, which we will neglect as it is smaller than the typical scale of the nucleon structure. So, the prescription to build the operators in the Lagrangian at nucleon level is,

$$\begin{aligned}
m_q\, \bar{q}q &\rightarrow f_{SN}^{(q)}\, m_N\, \hat{\bar{\psi}}_N\hat{\psi}_N \\
\bar{q}\gamma_\rho q &\rightarrow f_{VN}^{(q)}\, \hat{\bar{\psi}}_N\gamma_\rho\hat{\psi}_N \\
\frac{\beta_L}{2g_L^3}GG &\rightarrow f_{GN}\, m_N\, \hat{\bar{\psi}}_N\hat{\psi}_N .
\end{aligned} \tag{9}$$

The energy-momentum tensor relation for light quarks (Eq. (2)) and the fact that $\langle N|\theta_\alpha^\alpha|N\rangle = m_N\, \bar{\psi}_N\psi_N$ imply the simple sum-rule

$$1 = \sum_{q=u,d,s} f_{SN}^{(q)} + f_{GN} \ , \tag{10}$$

which we use to eliminate the form-factore f_{GN} in terms of the scalar nucleon form factors $f_{SN}^{(q)}$. The nucleon vector form factors are known from the vector current conservation,

$$\begin{array}{ll}
f_{Vp}^{(u)} = 2 & f_{Vn}^{(u)} = 1 \\
f_{Vp}^{(d)} = 1 & f_{Vn}^{(d)} = 2 \\
f_{Vp}^{(s)} = 0 & f_{Vn}^{(s)} = 0
\end{array} , \tag{11}$$

while the calculation of the scalar form factors $f_{SN}^{(q)}$ is non-trivial. As discussed below, in our analysis we will use input from Chiral Perturbation Theory and the lattice to asses the impact of current and future uncertainties on the conversion rate.
Collecting the above results, the Lagrangian at nucleon level can be written as

$$\begin{aligned}\mathcal{L}_{eff}^{(N)} &= -\frac{1}{\Lambda^2}\sum_{N=p,n}\Big[\left(C_{DR}m_\mu\,\bar{e}\sigma^{\rho\nu}\mathcal{P}_L\mu + C_{DL}m_\mu\,\bar{e}\sigma^{\rho\nu}\mathcal{P}_R\mu\right)F_{\rho\nu} \\ &+ \left(\tilde{C}_{VR}^{(N)}\,\bar{e}\gamma^\rho\mathcal{P}_R\mu + \tilde{C}_{VL}^{(N)}\,\bar{e}\gamma^\rho\mathcal{P}_L\mu\right)\hat{\bar{\psi}}_N\gamma_\rho\hat{\psi}_N \\ &+ G_F m_\mu m_N\left(\tilde{C}_{SR}^{(N)}\,\bar{e}\mathcal{P}_L\mu + \tilde{C}_{SL}^{(N)}\,\bar{e}\mathcal{P}_R\mu\right)\hat{\bar{\psi}}_N\hat{\psi}_N + h.c.\Big]\,. \end{aligned} \tag{12}$$

The new effective couplings $\tilde{C}$ not only contain the information about the underlying theory, but also about the hadronization. The vector couplings are:

$$\tilde{C}_{VR}^{(p)} = \sum_{q=u,d,s} C_{VR}^{(q)} f_{Vp}^{(q)} \tag{13}$$

$$\tilde{C}_{VR}^{(n)} = \sum_{q=u,d,s} C_{VR}^{(q)} f_{Vn}^{(q)} \tag{14}$$

$$\tilde{C}_{VL}^{(p)} = \sum_{q=u,d,s} C_{VL}^{(q)} f_{Vp}^{(q)} \tag{15}$$

$$\tilde{C}_{VL}^{(n)} = \sum_{q=u,d,s} C_{VL}^{(q)} f_{Vn}^{(q)}\,, \tag{16}$$

while the scalar ones read:

$$\tilde{C}_{SR}^{(p)} = \sum_{q=u,d,s} C_{SR}^{(q)} f_{Sp}^{(q)} + C_{GQR}\,(1 - \sum_{q=u,d,s} f_{Sp}^{(q)}) \tag{17}$$

$$\tilde{C}_{SR}^{(n)} = \sum_{q=u,d,s} C_{SR}^{(q)} f_{Sn}^{(q)} + C_{GQR}\,(1 - \sum_{q=u,d,s} f_{Sn}^{(q)}) \tag{18}$$

$$\tilde{C}_{SL}^{(p)} = \sum_{q=u,d,s} C_{SL}^{(q)} f_{Sp}^{(q)} + C_{GQL}\,(1 - \sum_{q=u,d,s} f_{Sp}^{(q)}) \tag{19}$$

$$\tilde{C}_{SL}^{(n)} = \sum_{q=u,d,s} C_{SL}^{(q)} f_{Sn}^{(q)} + C_{GQL}\,(1 - \sum_{q=u,d,s} f_{Sn}^{(q)})\,. \tag{20}$$

2.4 Transition rates

The nucleon-level effective lagrangian can be used to take matrix elements at the atomic and nuclear level. In the non-relativistic approximation, the relevant matrix elements are

$$\begin{aligned}
\langle A,Z|\bar{\psi}_p\psi_p|A,Z\rangle &= Z\rho^{(p)} \\
\langle A,Z|\bar{\psi}_n\psi_n|A,Z\rangle &= (A-Z)\rho^{(n)} \\
\langle A,Z|\bar{\psi}_p\gamma^0\psi_p|A,Z\rangle &= Z\rho^{(p)} \\
\langle A,Z|\bar{\psi}_n\gamma^0\psi_n|A,Z\rangle &= (A-Z)\rho^{(n)} \\
\langle A,Z|\bar{\psi}_N\gamma^i\psi_N|A\rangle &= 0\,.
\end{aligned} \tag{21}$$

Here $|A,Z\rangle$ represents the nuclear ground state, with A and Z the mass and atomic number of the isotope, while $\rho^{(p)}$ and $\rho^{(n)}$ are the proton and neutron densities respectively. The conversion rate of the process is written as

$$\begin{aligned}
\Gamma_{conv} &= \frac{m_\mu^5}{4\Lambda^4}\left|C_{DR}\,D + 4G_F m_\mu\left(m_p\tilde{C}_{SR}^{(p)}S^{(p)} + m_n\tilde{C}_{SR}^{(n)}\,S^{(n)}\right) + \tilde{C}_{VR}^{(p)}\,4V^{(p)} + \tilde{C}_{VR}^{(n)}\,4V^{(n)}\right|^2 \\
&+ \frac{m_\mu^5}{4\Lambda^4}\left|C_{DL}\,D + 4G_F m_\mu\left(m_p\tilde{C}_{SL}^{(p)}S^{(p)} + m_n\tilde{C}_{SL}^{(n)}\,S^{(n)}\right) + \tilde{C}_{VL}^{(p)}\,4V^{(p)} + \tilde{C}_{VL}^{(n)}\,4V^{(n)}\right|^2
\end{aligned} \tag{22}$$

in terms of the dimensionless integrals $D, V^{(N)}, S^{(N)}$, representing the overlap of electron and muon wavefunctions weighted by appropriate combinations of protons and neutron densities [1]. For completeness, we report the expressions of the overlap integrals in Appendix. For phenomenological applications, it is useful to normalize the conversion rate to the muon capture rate, introducing the quantity:

$$B_{\mu\to e}(Z) \equiv \frac{\Gamma_{conv}(Z,A)}{\Gamma_{capt}(Z,A)}\,. \tag{23}$$

Finally, we note here the branching ratio for the purely radiative process $\mu \to e\gamma$ in terms of the effective couplings defined above:

$$B_{\mu\to e\gamma} \equiv \frac{\Gamma(\mu\to e\gamma)}{\Gamma(\mu\to e\nu_\mu\bar{\nu}_e)} = \frac{48\pi^2}{4\,G_F^2\,\Lambda^4}\,\left(|C_{DR}|^2 + |C_{DL}|^2\right)\,. \tag{24}$$

2.5 Sources of uncertainty

There are two sources of uncertainty in the calculation of the transition rate: (i) scalar form factors and (ii) neutron density (for high Z nuclei). The latter uncertainty has been carefully discussed in Ref. [1], where several approaches to determine the neutron density have been reviewed and used in the calculation of the overlap integrals. Whenever data from polarized proton scattering exists, the uncertainty on the overlap integrals $S^{(n)}$ and $V^{(n)}$ can be reduced to a few percent even for heavy nuclei such as Pb. Otherwise, it should

be considered to be of the order of 10%.
In this work we focus on the uncertainty induced in the hadronization process, namely the scalar density matrix elements in the nucleon.

The scalar form factors defined in Eq. 8 can be re-expressed in terms of ratio of quark masses and ratios of nucleon matrix elements as follows [5]:

$$f_{Sp}^{(u)} = \frac{m_u}{m_u + m_d}(1+\xi)\frac{\sigma_{\pi N}}{m_p} \tag{25}$$

$$f_{Sp}^{(d)} = \frac{m_d}{m_u + m_d}(1-\xi)\frac{\sigma_{\pi N}}{m_p} \tag{26}$$

$$f_{Sp}^{(s)} = \frac{m_s}{m_u + m_d} y \frac{\sigma_{\pi N}}{m_p} \tag{27}$$

$$f_{Sn}^{(u)} = \frac{m_u}{m_u + m_d}(1-\xi)\frac{\sigma_{\pi N}}{m_p} \tag{28}$$

$$f_{Sn}^{(d)} = \frac{m_d}{m_u + m_d}(1+\xi)\frac{\sigma_{\pi N}}{m_p} \tag{29}$$

$$f_{Sn}^{(s)} = \frac{m_s}{m_u + m_d} y \frac{\sigma_{\pi N}}{m_p} , \tag{30}$$

where

$$\sigma_{\pi N} = \frac{m_u + m_d}{2}\langle p|\bar{u}u + \bar{d}d|p\rangle \tag{31}$$

$$\xi = \frac{\langle p|\bar{u}u - \bar{d}d|p\rangle}{\langle p|\bar{u}u + \bar{d}d|p\rangle} \tag{32}$$

$$y = \frac{2\langle p|\bar{s}s|p\rangle}{\langle p|\bar{u}u + \bar{d}d|p\rangle} . \tag{33}$$

Information on the above matrix elements can be obtained either by the analysis of the octet baryon masses within Heavy Baryon Chiral Perturbation Theory, or by Lattice QCD. Especially for the ratio denoted here with y, the determination is still somewhat controversial.

For the σ-term, we will use the range [9]:

$$\sigma_{\pi N} = (49 \pm 3)\,\text{MeV} , \tag{34}$$

while for the ratio measuring isospin-breaking, we will use [5, 10]:

$$\xi = 0.132 \pm 0.035 . \tag{35}$$

For the ratio y quantifying the strange quark content of the nucleon, the situation is less clear. A Chiral Perturbation Theory analysis gives the range $y = 0.21 \pm 0.2$ [11]. The large uncertainty reflects the poor knowledge of the relevant low-energy constants, even within resonance saturation (the matching renormalization scale is arbitrary). A recent lattice QCD analysis [12] with two dynamical flavors (in the overlap fermion formulation

with good chiral symmetry behavior) results in the central value $y \sim 0.05$, still consistent with the Chiral Perturbation Theory range. The difference with respect to previous lattice results has been attributed to a lattice artifact (mixing with wrong chirality operator) in the Wilson fermion approach.

For the purpose of this work, we will vary the parameter y within both a "conservative" range and an "optimistic" range. For the conservative range we take $y \in [0, 0.4]$, which coincides with the ChPT range of Ref [11]. For the optimistic range we take $y \in [0, 0.05]$ which reflects more closely the recent JLQCD result [12] and seems a realistic guess of the uncertainty that will be reached by lattice calculations in the next decade.

Finally, for the ratios of quark masses, we still use the the input [13]:

$$\frac{m_u}{m_d} = 0.553 \pm 0.043 \tag{36}$$

$$\frac{m_s}{m_d} = 18.9 \pm 0.8 \tag{37}$$

3 Testing the single operator dominance hypothesis

We now turn to illustrate the model discriminating power of a combined phenomenological analysis of $\mu \to e\gamma$ and $\mu \to e$ conversion on different target nuclei. In order to organize the discussion, we define here four classes of models, in which only one underlying short distance operator dominates over all the others. We call these four classes of models the "single-operator" dominance models. We will first analyze this simplest class of models and then consider the more involved case in which two operators have comparable strengths and interference effects cannot be neglected.

3.1 Dipole, Vector and Scalar models

- **Dipole model**

  The Dipole model is defined by the assumption that, among all LFV short-distance operators, the dipole operator is the dominant one. For simplicity, we focus on the case in which the outgoing lepton has definite chirality. Explicitly, in terms of the effective couplings defined in Eq. 1, this class of models is defined by:

  $$C_D \equiv C_{DR} \neq 0 \quad C_{else} = 0 \quad . \tag{38}$$

  Most supersymmetric scenarios, including SUSY-GUT models [14] and SUSY see-saw models [15] fall in this class of models.

- **Vector model 1:** $V(\gamma)$

  This model is defined by the assumption that the transition charge radius operator gives the dominant contribution to the LFV lagrangian. The model is defined by:

  $$C_V \equiv C_{VR}^{(u)} \neq 0 \quad C_{VR}^{(d)} = -\tfrac{1}{2}\, C_{VR}^{(u)} \quad C_{else} = 0 \, . \tag{39}$$

- **Vector model 2:** $V(Z)$

  The Vector model 2 is defined by the assumption that the underlying dominant operator is an effective Z-penguin. The ratios of couplings of different quarks is governed by the couplings of the Z^0 coupling to quarks. The model is defined by:

$$C_V \equiv C_{VR}^{(u)} \neq 0 \quad C_{VR}^{(d)} = a\, C_{VR}^{(u)} \quad C_{else} = 0\,, \tag{40}$$

  where a is the ratio of the *down* and *up* quarks coupling to the Z-boson:

$$a = \frac{T_{d_L}^3 + T_{d_R}^3 - (Q_{d_L} + Q_{d_R}) sin^2\theta_W}{T_{u_L}^3 + T_{u_R}^3 - (Q_{u_L} + Q_{u_R}) sin^2\theta_W} = -1.73\,. \tag{41}$$

- **Scalar model**

  This model is defined by:

$$C_S \equiv C_{SR}^{(d)} = C_{SR}^{(s)} = C_{SR}^{(b)} \quad C_{else} = 0\,. \tag{42}$$

  This model may be explicitly realized in some regions of the usual R-parity conserving SUSY see-saw parameter space [16] (large $\tan\beta$ and relatively low "heavy" Higgs sector) and within R-parity violating SUSY [17].

Each of the above classes of models has only one free parameter – the ratio C_i/Λ^2 of the dominant effective coupling over the square of the new physics scale. It is clear, then, that the single-operator dominance hypothesis makes parameter-free predictions for ratios of LFV branching fractions and therefore it can be tested so long as two LFV rates are measured.

3.2 $\mu \to e\gamma$ vs $\mu \to e$ conversion

If $\mu \to e\gamma$ and $\mu \to e$ conversion in at least one target nucleus are observed, this immediately opens up the possibility to test the Dipole dominance model. In fact, in this model the ratio

$$R(Z) = \frac{B_{\mu\to e}(Z)}{B_{\mu\to e\gamma}} \tag{43}$$

is entirely fixed by the overlap integrals D [1], which are essentially free of theoretical uncertainty. $R(Z)$ is predicted to scale as $\mathcal{O}(\alpha/\pi)$ and we plot it in Fig. 1. Any deviation from this pattern implies the presence of scalar or/and vector contributions. In order to disentangle these possibilities, one needs to study the target dependence of the conversion rate.

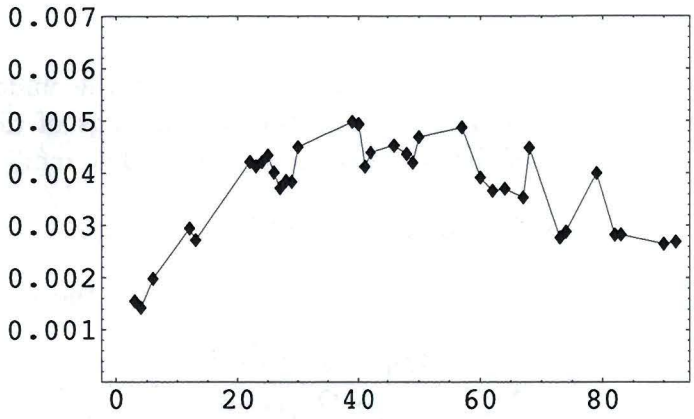

Figure 1: Ratio $R(Z)$ of $\mu \to e$ conversion over $B(\mu \to e\gamma)$ versus Z in the case of Dipole dominance model.

3.3 Target dependence of $\mu \to e$ conversion

In principle, any single-operator model can be tested with two conversion rates, even if $\mu \to e\gamma$ is not observed. To illustrate this point, we update the analysis of Ref. [1] and plot in Fig. 2 the conversion rate (normalized to the rate in Aluminum) as a function of the Z of the target nucleus, for the four classes of single-operator models defined above. Compared to Ref. [1], the novelty here is the inclusion of a second vector model ($V(Z)$) and the fact that we consider only those target nuclei in which the process of muon capture followed by gamma emission produces electrons that do not overlap with the signal region [18] (a necessary condition for the measurement).

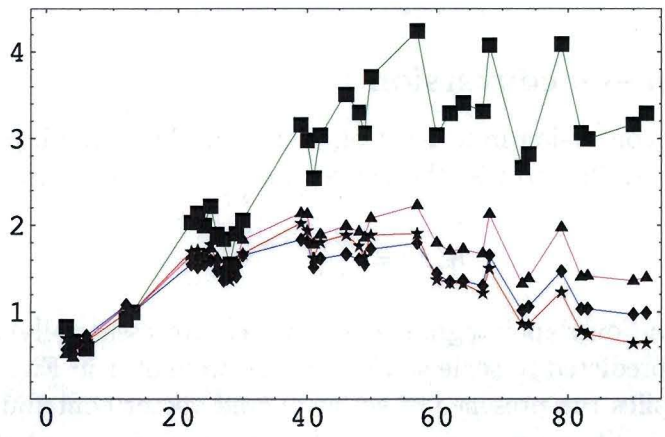

Figure 2: Target dependence of the $\mu \to e$ conversion rate in different single-operator dominance models. We plot the conversion rates normalized to the rate in Aluminum (Z=13) versus the atomic number Z for the four theoretical models described in the text: D (blue), S (red), $V(\gamma)$ (magenta), $V(Z)$ (green). **Remove the "spikes"? (Au,...)**

The results of Fig. 2 show some noteworthy features. First, we note the quite different target dependence of the conversion rate in the two vector models considered. This can be understood as follows: in the case of the $V(\gamma)$ model, the behavior in Fig. 2 simply traces the Z-dependence of $V^{(p)}$ (the photon only couples to the protons in the nucleus). On the other hand, in the case of the $V(Z)$ model, the Z boson couples predominantly to the neutrons in the nucleus and the residual target dependence of the ratio $V^{(n)}/V^{(p)}$ generates the behavior observed in Fig. 2.

Next, let us focus on the actual discriminating power of the Z-dependence. Clearly, the plot shows that the model-discriminating power tends to increase with Z. This is a simple reflection of the fact that the whole effect is of relativistic origin and increases in heavy nuclei. So in an ideal world, in order to maximize the chance to discriminate among underlying models, one would like to measure the conversion rate in a lignt nucleus, say Aluminum or Titanium, as well as in a large-Z nucleus, like Lead or Gold. This simplified view, however, has to be confronted both with theoretical uncertainties and the actual experimental feasibility. Concerning the uncertainties, a simple analysis shows that the dominant uncertainty coming from the scalar matrix elements almost entirely cancels when taking ratios of conversion rates (even using the conservative range $y \in [0, 0.4]$ for the strange scalar density matrix element. Moreover, in the large-Z tail of the plot, some residual uncertainty arises from the input on the neutron density profile. When polarized proton scattering data exists, the uncertainty on the ratios of conversion rates becomes negligible. This point is illustrated by Table 1, where we report the detailed breakdown of uncertainties in the ratios $B_{\mu\to e}(Ti)/B_{\mu\to e}(Al)$ and $B_{\mu\to e}(Pb)/B_{\mu\to e}(Al)$. For other targets, the uncertainty induced by neutron densities never exceeds 5% [1]. The conclusions of this exercise are that:

- In tests of the single-operator dominance models, the theoretical uncertainties (scalar matrix elements and neutron densities) largely cancel.
- As evident from Fig.. 2, a realistic discrimination among models requires a measure of $B_{\mu\to e}(Ti)/B_{\mu\to e}(Al)$ at the level of 5% or better, or alternatively a measure of $B_{\mu\to e}(Pb)/B_{\mu\to e}(Al)$ at the 20% level. These are two cases that well represent the trend in light and heavy target nuclei.

4 Testing the two-operator dominance hypothesis

In the last section we have discussed how to test the hypothesis of a single operator dominance, and how to discriminate among different single-operator dominance models. If the single operator dominance hypothesis fails, one is lead to consider next simplest case, namely the two-operator dominance models, defined by the assumption that only two underlying operators have appreciable coefficients. Each model is characterized by two parameters, the effective strength C_1/Λ^2 of one of the two operators and the ratio C_2/C_1 of the effective couplings of the two dominant operators. This class of models can be tested so long as two double ratios of LFV rates is available (three LFV measurements!).

	S	D	V(γ)	V(Z)
$\frac{B(\mu\to e,Ti)}{B(\mu\to e,Al)}$	1.70 $\pm$ 0.005	1.55	1.65	2.0
$\frac{B(\mu\to e,Pb)}{B(\mu\to e,Al)}$	0.69 $\pm$ 0.02	1.04	1.41	2.67 $\pm$ 0.06

Table 1: Ratios of conversion rates in Titanium and Lead over Aluminum, in each of the four single-operator models: scalar (S), dipole (D), vector 1 (photon coupling to the quarks) and vector 2 (Z boson coupling to the quarks). In the scalar model, the scalar form factor induces a negligible uncertainty in the ratios involving two targets. In the case of Lead over Aluminum, the small uncertainty is dominated by the neutron density input.

For the sake of illustration, we will consider the following three two-operator models: Dipole-Scalar, Dipole-Vector(Z) and Scalar-Vector(Z). We consider both the case of constructive and destructive interference among the two dominant operators, assuming that the ratio of Wilson coefficients $r \equiv C_2/C_1$ is real (a relative phase can be included but it would unnecessary complicate the analysis at this early stage).
In order to test this class of models, one has to assume that at least three LFV processes have been observed, so one can construct two independent double ratios that are entirely determined by the single parameter r. In models involving the Dipole operator among the dominant terms (such as Dipole-Scalar and Dipole-Vector) the three observables could be (i) $\mu \to e\gamma$ and $\mu \to e$ conversion in two different targets; (ii) $\mu \to e$ conversion in three different targets. In models that do not involve a Dipole term (such as Scalar-Vector), only the possibility (ii) above is available. As representative target nuclei, we have chosen aluminum (Al), titanium (Ti), and lead (Pb).

4.1 Dipole-Scalar

In terms of the parameters defined in Section 3.1, this model is defined by $C_S \neq 0$ and $C_D \equiv \pm\frac{r}{8e}\, C_S$. Clearly, in the limiting cases $r \to 0$ and $r \to \infty$ one recovers the single-operator models.

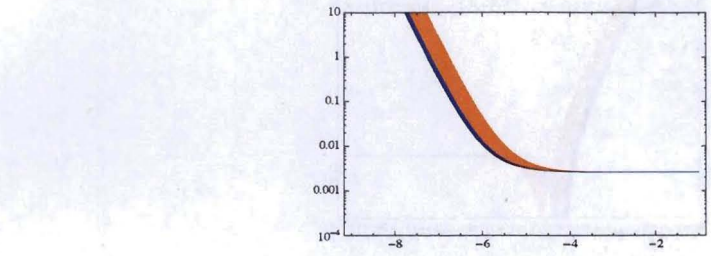

(a)

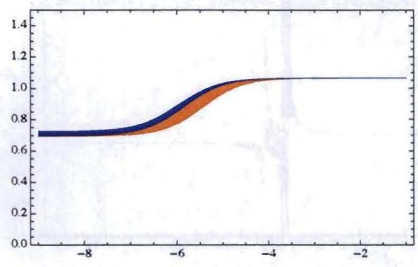

(b)

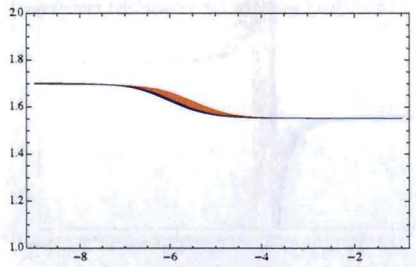

(c)

Figure 3: *Dipole-Scalar model*: Ratios $B_{\mu\to e}(Al)/B_{\mu\to e\gamma}$ (panel (a)), $B_{\mu\to e}(Pb)/B_{\mu\to e}(Al)$ (panel (b)), and $B_{\mu\to e}(Ti)/B_{\mu\to e}(Al)$ (panel (c)) as a function of $\mathrm{Log}_{10}(r)$ for positive C_D/C_S. See text for details.

We illustrate the features of this model in Figs. 3 and 4, which correspond to positive and negative sign of the ratio C_D/C_S, respectively. Panel (a) shows the behavior of $B_{\mu\to e}(Al)/B_{\mu\to e\gamma}$ versus the parameter r, while panels (b) and (c) show the ratios $B_{\mu\to e}(Pb)/B_{\mu\to e}(Al)$ and $B_{\mu\to e}(Ti)/B_{\mu\to e}(Al)$, respectively. In panels (a) and (c) the curve is widened in the interference region by the uncertainty in the scalar form factors. The dominant uncertainty comes form the input parameter y, characterizing the strangeness content of the nucleon. On the other hand, the ratio $B_{\mu\to e}(Pb)/B_{\mu\to e}(Al)$ is affected not only by the uncertainty in the scalar form factors, but also by the uncertainty induced in the overlap integral by the neutron density in Pb. The width of the bands in panel (b) is determined by the most conservative combination of two kind of uncertainties.

In all panels the wide band corresponds to the range $y \in [0, 0.4]$, while the narrow band corresponds to the range $y \in [0, 0.05]$. This illustrates the effect of current and future hadronic uncertainties on the process of extracting information on short distance LFV couplings. The prominent feature in Fig. 4 is induced by the destructive interference dipole and scalar amplitudes.

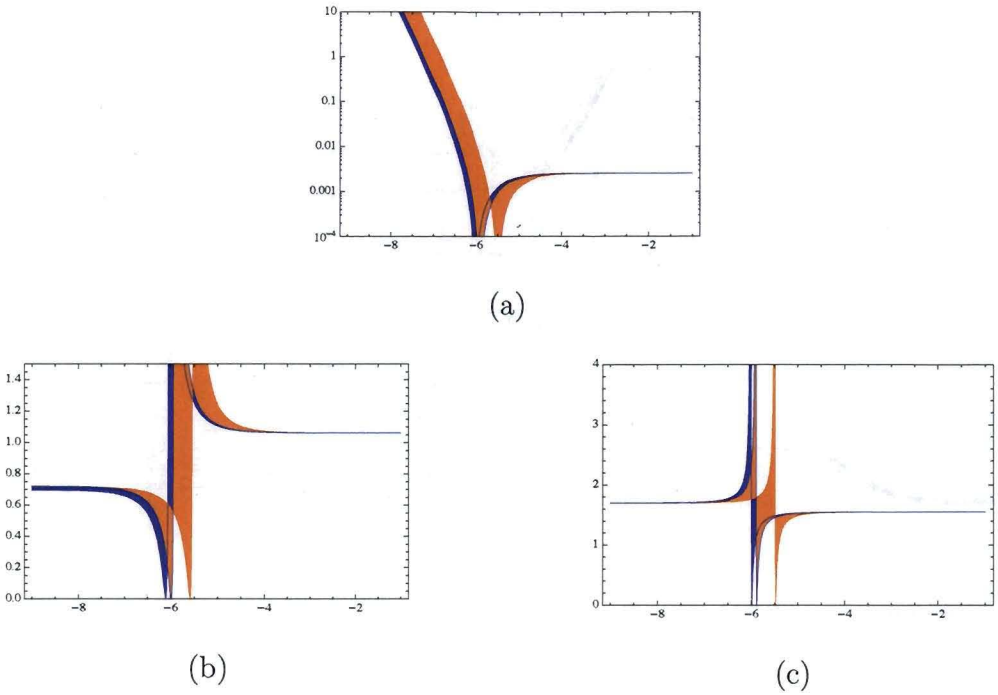

Figure 4: *Dipole-Scalar model*: Ratios $B_{\mu\to e}(Al)/B_{\mu\to e\gamma}$ (panel (a)), $B_{\mu\to e}(Pb)/B_{\mu\to e}(Al)$ (panel (b)), and $B_{\mu\to e}(Ti)/B_{\mu\to e}(Al)$ (panel (c)) as a function of $\mathrm{Log}_{10}(r)$ for negative C_D/C_S. See text for details.

4.2 Dipole-Vector

In terms of the parameters defined in Section 3.1, this model is defined by $C_V \neq 0$ and $C_D \equiv \pm\frac{r}{8e}\, C_V$. In figures 5 and 6 we plot the ratios $B_{\mu\to e}(Al)/B_{\mu\to e\gamma}$ (panel (a)), $B_{\mu\to e}(Pb)/B_{\mu\to e}(Al)$ (panel (b)), and $B_{\mu\to e}(Ti)/B_{\mu\to e}(Al)$ (panel (c)) versus the parameter r. Figures 5 and 6 correspond to positive and negative sign of the ratio C_D/C_V, respectively. Within this model, the only source of uncertainty arises from the vector overlap integral $V^{(n)}(Pb)$, sensitive to the neutron density in Pb. This uncertainty is quantified by the thickness of the band in panel (b).

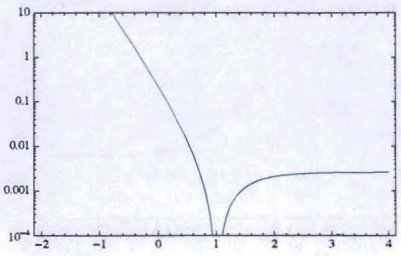

(a)

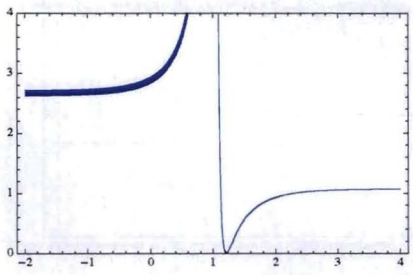

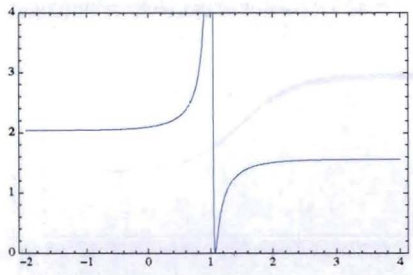

(b) (c)

Figure 5: *Dipole-Vector model*: Ratios $B_{\mu\to e}(Al)/B_{\mu\to e\gamma}$ (panel (a)), $B_{\mu\to e}(Pb)/B_{\mu\to e}(Al)$ (panel (b)), and $B_{\mu\to e}(Ti)/B_{\mu\to e}(Al)$ (panel (c)) as a function of $\mathrm{Log}_{10}(r)$ for positive C_D/C_V. See text for details.

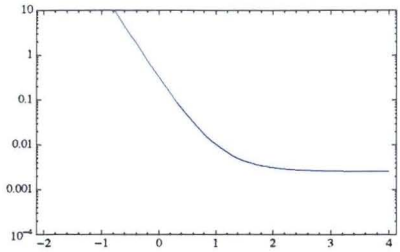

(a)

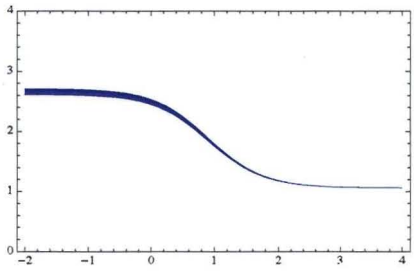

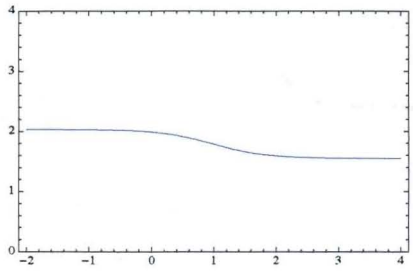

(b) (c)

Figure 6: *Dipole-Vector model*: Ratios $B_{\mu\to e}(Al)/B_{\mu\to e\gamma}$ (panel (a)), $B_{\mu\to e}(Pb)/B_{\mu\to e}(Al)$ (panel (b)), and $B_{\mu\to e}(Ti)/B_{\mu\to e}(Al)$ (panel (c)) as a function of $\mathrm{Log}_{10}(r)$ for negative C_D/C_V. See text for details.

4.3 Scalar-Vector

In terms of the parameters defined in Section 3.1, this model is defined by $C_V \neq 0$ and $C_S \equiv \pm r\, C_V$. Since the Dipole term is assumed to be subdominant, in this case we include in the analysis only the ratios $B_{\mu\to e}(Pb)/B_{\mu\to e}(Al)$ and $B_{\mu\to e}(Ti)/B_{\mu\to e}(Al)$, shown in panels (b) and (c) of Figures 7 and 8 (for positive and negative values of C_S/C_V, respectively). While the ratio $B_{\mu\to e}(Ti)/B_{\mu\to e}(Al)$ is affected only by the uncertainty in y, the ratio $B_{\mu\to e}(Pb)/B_{\mu\to e}(Al)$ is affected also by the uncertainty in the Pb neutron density (through the overlap integrals). The width of the bands in the plots is determined by the most conservative combination of two kind of uncertainties.

In all panels the wide band corresponds to the range $y \in [0, 0.4]$, while the narrow band corresponds to the range $y \in [0, 0.05]$. As in the case of the Dipole-Scalar model, the bands illustrate the effect of current and future hadronic uncertainties on extracting short distance LFV couplings.

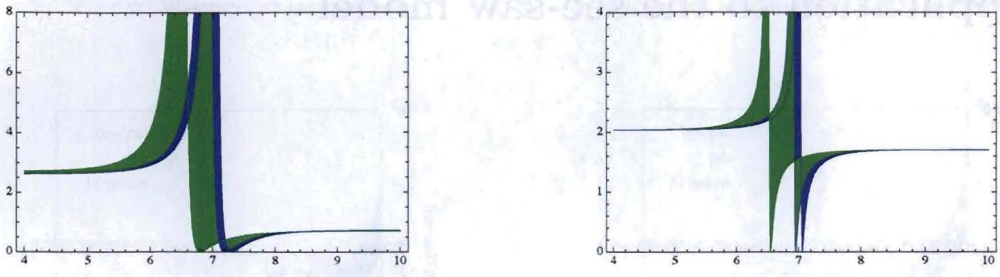

(b) (c)

Figure 7: *Scalar-Vector model*: Ratios $B_{\mu\to e}(Pb)/B_{\mu\to e}(Al)$ (panel (b)) and $B_{\mu\to e}(Ti)/B_{\mu\to e}(Al)$ (panel (c)) as a function of $\mathrm{Log}_{10}(r)$ for positive C_S/C_V. See text for details.

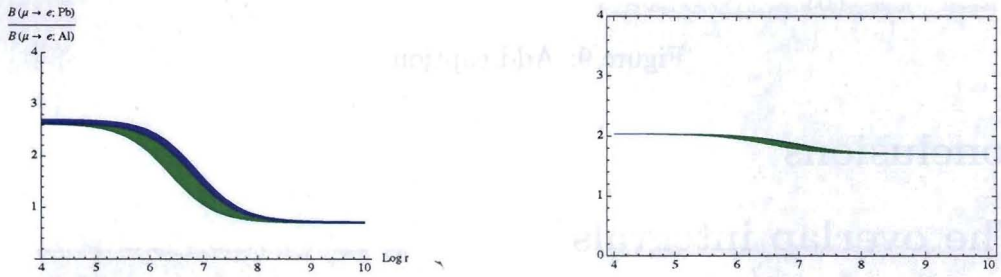

(b) (c)

Figure 8: *Scalar-Vector model*: Ratios $B_{\mu\to e}(Pb)/B_{\mu\to e}(Al)$ (panel (b)) and $B_{\mu\to e}(Ti)/B_{\mu\to e}(Al)$ (panel (c)) as a function of $\mathrm{Log}_{10}(r)$ for negative C_S/C_V. See text for details.

We conclude this section by summarizing what one could learn about the two-operator dominance models in the case that two double ratios of LFV rates could be measured experimentally. Our exercise shows that:

- The current theoretical uncertainty on the strange content of the nucleon prevents a realistic test of the two-operator models involving the Scalar amplitude. The range $y \in [0, 0.4]$ induces uncertainties of up to one order of magnitude in the relevant double ratios in the interference region (thick bands in all plots above). However, the uncertainty within reach of lattice QCD calculations will remove this obstacle in the coming years (this is illustrated by the thin bands in all plots above).

- Testing and discriminating among two-operator dominance models requires an experimental precision on the LFV rates that is comparable to the one needed to test the single operator models.

5 Application to the see-saw model

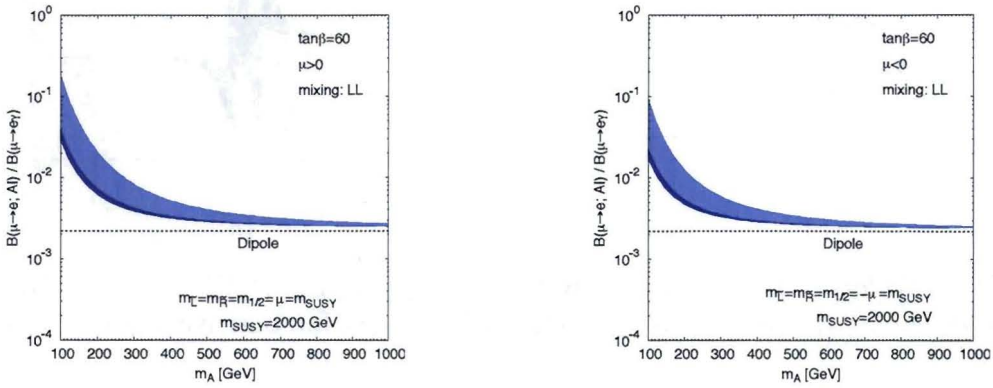

(b) (c)

Figure 9: Add caption.

6 Conclusions

A The overlap integrals

The initial state in the μ-e conversion process is the $1s$ state of the muonic atom and the final electron state is the the ground state of the resulting nucleus, with an out going electron of energy $m_\mu - \epsilon_b$, where ϵ_b is the binding energy of the $1s$ muonic atom. The lepton wave-functions are determined by solving the Dirac equation in the electric field of the nucleus [1]. They are characterized by $-\kappa$ and μ quantum numbers, which are eigenvalues of two operators that commute with the Hamiltonian, K and the third component of the angular momentum, j_z, respectively. Those functions are easily written following the procedure of R. Kitano *et al.* [1]:

$$\Psi_{(\mu)}(r,\theta,\phi) = \begin{pmatrix} g^-_{(\mu)}(r)\chi^{\pm 1/2}_{-1}(\theta,\phi) \\ if^-_{(\mu)}(r)\chi^{\pm 1/2}_{1}(\theta,\phi) \end{pmatrix}, \tag{44}$$

$$\Psi_{(e)}(r,\theta,\phi) = \begin{pmatrix} g^-_{(e)}(r)\chi^{\pm 1/2}_{-1}(\theta,\phi) \\ if^-_{(e)}(r)\chi^{\pm 1/2}_{1}(\theta,\phi) \end{pmatrix}, \tag{45}$$

$$\Psi_{(e)}(r,\theta,\phi) = \begin{pmatrix} g^+_{(e)}(r)\chi^{\pm 1/2}_{1}(\theta,\phi) \\ if^+_{(e)}(r)\chi^{\pm 1/2}_{-1}(\theta,\phi) \end{pmatrix}. \tag{46}$$

The initial muon wave function (44) corresponds to the quantum numbers $\mu = \pm 1/2$ and $\kappa = -1$, while the final electron state, (45) and (46), is one of the states in the continuum spectrum and its wave functions can be $\kappa = \pm 1$. They are normalized as follows:

$$\int d^3x \Psi^*_{(\mu)}(x)\Psi_{(\mu)}(x) = 1 \,, \tag{47}$$

$$\int d^3x \Psi^{\mu *}_{(e)\kappa,W}(x)\Psi^{\mu'}_{(e)\kappa',W'}(x) = 2\pi\delta_{\mu\mu'}\delta_{\kappa\kappa'}\delta(W - W') \,. \tag{48}$$

In terms of the wafe-functions defined above, the overlap integrals have the following expressions [1]:

$$\begin{aligned}
m_\mu^{5/2} D &= \frac{4}{\sqrt{2}} m_\mu \int_0^\infty dr\, r^2 [-E(r)](g^-_{(e)} f^-_{(\mu)} + f^-_{(e)} g^-_{(\mu)}) \\
m_\mu^{5/2} S^{(p)} &= \frac{1}{2\sqrt{2}} \int_0^\infty dr\, r^2 Z\rho^{(p)}(g^-_{(e)} g^-_{(\mu)} - f^-_{(e)} f^-_{(\mu)}) \\
m_\mu^{5/2} S^{(n)} &= \frac{1}{2\sqrt{2}} \int_0^\infty dr\, r^2 (A-Z)\rho^{(n)}(g^-_{(e)} g^-_{(\mu)} - f^-_{(e)} f^-_{(\mu)}) \\
m_\mu^{5/2} V^{(p)} &= \frac{1}{2\sqrt{2}} \int_0^\infty dr\, r^2 Z\rho^{(p)}(g^-_{(e)} g^-_{(\mu)} + f^-_{(e)} f^-_{(\mu)}) \\
m_\mu^{5/2} V^{(n)} &= \frac{1}{2\sqrt{2}} \int_0^\infty dr\, r^2 (A-Z)\rho^{(n)}(g^-_{(e)} g^-_{(\mu)} + f^-_{(e)} f^-_{(\mu)}) \,.
\end{aligned} \tag{49}$$

Here the electric field, $E(r)$, is obtained by integrating Maxwell's equations as

$$E(r) = \frac{Ze}{r^2} \int_0^r r'^2 \rho^{(p)}(r')\, dr' \,. \tag{50}$$

The electric potential is obtained from $E(r)$ as follows,

$$V(r) = -e \int_r^\infty E(r')\, dr' \,. \tag{51}$$

References

[1] R. Kitano, M. Koike and Y. Okada, Phys. Rev. D **66**, 096002 (2002) [Erratum-ibid. D **76**, 059902 (2007)] [arXiv:hep-ph/0203110].

[2] T. P. Cheng, Phys. Rev. D 38, 2869 (1988);
H. Cheng, Phys. Lett. B 219, 347 (1989).

[3] T. S. Kosmas, S. Kovalenko and I. Schmidt, Phys. Lett. B 511, 203 (2001).

[4] V. Cirigliano, B. Grinstein, G. Isidori and M. B. Wise, Nucl. Phys. B 729, 121-134 (2005).

[5] A. Corsetti and P. Nath, Phys. Rev. D **64**, 125010 (2001) [arXiv:hep-ph/0003186].

[6] H. Ohki, H. Fukaya, S. Hashimoto, T. Kaneco, H. Matsufuru, J. Noaki, T. Onogi, E. Shintani and Y. Yamada, arXiv:0806.4744.

[7] S. J. Dong, J. -F. Lagaë and K. F. Liu, Phys. Rev. D 54, 5496-5500 (1996).

[8] M. Fukugita, Y. Kuramashi, M. Okawa and A. Ukawa, Phys. Rev. D 51, 5319-5322 (1995).

[9] M. Procura, T. R. Hemmert and W. Weise, Phys. Rev. D **69**, 034505 (2004) [arXiv:hep-lat/0309020].

[10] H. Cheng, Phys. Lett. **B219**, 347 (1989)s

[11] B. Borasoy and U. G. Meissner, Annals Phys. **254**, 192 (1997) [arXiv:hep-ph/9607432].

[12] H. Ohki *et al.*, arXiv:0806.4744 [hep-lat].

[13] H. Leutwyler, Phys. Lett. B **378**, 313 (1996) [arXiv:hep-ph/9602366].

[14] R. Barbieri and L. J. Hall, Phys. Lett. B **338**, 212 (1994) [arXiv:hep-ph/9408406];
R. Barbieri, L. J. Hall and A. Strumia, Nucl. Phys. B **445**, 219 (1995) [arXiv:hep-ph/9501334];
J. Hisano, T. Moroi, K. Tobe and M. Yamaguchi, Phys. Lett. B **391**, 341 (1997) [Erratum-ibid. B **397**, 357 (1997)] [arXiv:hep-ph/9605296].

[15] F. Borzumati and A. Masiero, Phys. Rev. Lett. **57**, 961 (1986);
J. Hisano, T. Moroi, K. Tobe and M. Yamaguchi, Phys. Rev. D **53**, 2442 (1996) [arXiv:hep-ph/9510309].

[16] See-saw model at large tan beta ....

[17] J. E. Kim, P. Ko and D. G. Lee, Phys. Rev. D **56**, 100 (1997) [arXiv:hep-ph/9701381];
K. Huitu, J. Maalampi, M. Raidal and A. Santamaria, Phys. Lett. B **430**, 355 (1998) [arXiv:hep-ph/9712249];
A. Faessler, T. S. Kosmas, S. Kovalenko and J. D. Vergados, Nucl. Phys. B **587**, 25 (2000);
A. de Gouvea, S. Lola and K. Tobe, Phys. Rev. D **63**, 035004 (2001) [arXiv:hep-ph/0008085].

[18] Mihara, private communication.